Available online at www.sciencedirect.com
ScienceDirect
Earth and Planetary Science Letters 250 (2006) 407–427
EPSL
www.elsevier.com/locate/epsl

Conflicting (U–Th)/He and fission track ages in apatite: Enhanced He retention, not anomalous annealing behaviour

Paul F. Green [a,*], Peter V. Crowhurst [b,1], Ian R. Duddy [a], Peter Japsen [c], Simon P. Holford [d]

[a] Geotrack International Pty Ltd., 37 Melville Rd., Brunswick West, Victoria, 3055, Australia
[b] CSIRO Petroleum Resources, Bentley 6151, WA, Australia
[c] Geological Survey of Denmark and Greenland (GEUS), Øster Voldgade 10, DK-1350 Copenhagen K, Denmark
[d] School of Geography, Earth and Environmental Sciences, University of Birmingham, Birmingham B15 2TT, United Kingdom

Received 3 March 2006; received in revised form 1 August 2006; accepted 23 August 2006
Available online 26 September 2006
Editor: G.D. Price

Abstract

While initial studies showed a high degree of consistency between AFTA and apatite (U–Th)/He dating, an increasing number of studies are reporting apatite (U–Th)/He ages which are older than expected on the basis of apatite fission track data from the same region. We present data from a range of geological settings to document a systematic discrepancy between the two systems, which becomes more pronounced in samples with older fission track ages (except for samples with very low uranium contents). Results from a granite pebble and enclosing volcanogenic sandstone provide a well-controlled test case in which independent constraints are available on the underlying thermal history. These demonstrate that the progressive discrepancy between the two techniques arises not from anomalous fission track annealing behaviour, as has been suggested, but as a result of a change in the He retention properties of apatite. This change appears to be linked to the degree of accumulated radiation damage within the crystal lattice, although underlying mechanisms remain unclear. We suggest detailed experiments should be performed to delineate and quantify the processes responsible. Until this is achieved, we suggest that apatite (U–Th)/He studies should also incorporate apatite fission track data, as well as other low temperature indicators, in order to monitor the (U–Th)/He system response and to guard against the anomalous behaviour described here.

Keywords: Thermochronology; AFTA; (U–Th)/He dating; apatite; fission track annealing; He diffusion; thermal history

1. Introduction

As the most recent addition to the armoury of low temperature thermochronological techniques, (U–Th)/He dating of apatite has rapidly found application in a variety of settings, providing novel insight into a wide range of topics [1–5]. Laboratory studies of He diffusion [6], combined with geological observations [7,8] have provided a detailed description of the sensitivity of (U–

* Corresponding author. Tel.: +61 3 9380 1077; fax: +61 3 9380 1477.
E-mail address: mail@geotrack.com.au (P.F. Green).
[1] Present address: Asia Pacific, Teck Cominco Australia Pty Ltd, Perth, WA, Australia.

0012-821X/$ - see front matter © 2006 Elsevier B.V. All rights reserved.
doi:10.1016/j.epsl.2006.08.022

Table 1
AFTA data, sample details and associated thermal history interpretations

Sample number	Map ref/ elevation	Location/ stratigraphic details[a]	ρ_D[b] (10^6 tracks/cm^2)	ρ_s[b] (10^6 tracks/cm^2)	ρ_i[b] (10^6 tracks/ cm^2)	Uranium content (ppm)	Zeta	$P(\chi^2)$ (%) (no. of grains	Fission track age[c] (Ma)	Mean track length[d] (μm)	Standard deviation (μm)	Thermal history constraints[e]
West Greenland												
GC861-2	750 m	Naujarssuit, Archean basement	1.111 (1742)	3.981 (1418)	4.169 (1485)	43	392.9±7.4	<1 (20)	201.9±19.5	13.15±0.18 (100)	1.84	>100 °C, 300–185 Ma 75–105 °C, 200–80 Ma 40–75 °C, 90–15 Ma
GC861-3	500 m	Naujarssuit, Archean basement	1.150 (1857)	3.512 (1611)	2.958 (1357)	29	392.9±7.4	1 (20)	260.0±15.1	13.10±0.22 (103)	2.25	110–115 °C, 290–210 Ma 60–80 °C, 190–80 Ma 40–70 °C, 135–20 Ma
GC861-4	5 m	Naujarssuit, Archean basement	1.118 (1742)	3.282 (1070)	3.798 (1238)	39	392.9±7.4	19 (20)	187.1±9.7	13.06±0.19 (104)	1.92	>115 °C, 245–195 Ma *70–100 °C, 200–140 Ma* <75 °C, 80–0 Ma
GC861-5	0 m	Inugsok, Archean basement	1.155 (1857)	2.183 (831)	2.675 (1018)	26	392.9±7.4	10 (20)	182.6±10.1	12.97±0.23 (106)	2.37	95–105 °C, 195–130 Ma 50–70 °C, 80–20 Ma
Yilgarn Block, Western Australia												
RD8-39 (W320)		Northam, WA (36°37′S, 116°34′E) Yilgarn Craton Archean basement	1.215 (1883)	4.273 (1030)	2.518 (607)	24	392.9±7.4	0.4 (20)	402.3±31.4	13.02±0.15 (103)	1.56	>100 °C, 500–380 Ma 65–75 °C, 240–100 Ma, <75 °C, 100–0 Ma
Cerberean Cauldron, Victoria												
8424-8 (RD8-30)	999457	Lake Mtn Rhyodacite, Cerberean Volcanics 375±1 Ma	1.080 (1657)	8.988 (3688)	6.968 (2859)	74	380.4±5.7	44 (19)	259.6±9.9	13.17±0.14 (53)	1.02	>105 °C, 320–270 Ma 50–70 °C, 120–0 Ma

Strangways Ranges, *Northern Territory*												
Ap1		Mud Tank Carbonatite, Central Australia (732±5 Ma)	1.123 (1761)	0.439 (492)	0.318 (356)	3.2	392.9±7.4	93 (20)	297.9±22.6	13.69±0.22 (92)	2.10	>100 °C, 380–270 Ma 50–85 °C, 280–90 Ma
Snowdon, *North Wales*												
RD35-23	SH577525 260 m	West flank of Snowdon, N Wales Ordovician (510–440 Ma)	1.085 (1629)	0.781 (738)	0.687 (649)	7.2	385.5±4.3	97 (19)	233.5±14.1	13.44±0.25 (52)	1.83	>105 °C, 305–220 Ma 85–105°C, 260–160 Ma 45–75 °C, 160–0 Ma
Otway Basin, *Victoria*												
RD14-339	969312 0 m	Shore platform, Kennett River, Victoria Aptian–Albian (120–105 Ma)	1.116 (1763)	0.352(379)	0.593 (639)	6.1	380.4±5.7	17 (20)	124.6±8.8	14.15±0.17 (64)	1.37	>75 °C, >50 Ma <70 °C, 85–0 Ma
RD14-341	969312 0 m	Shore platform, Kennett River, Victoria Aptian–Albian (120–105 Ma)	1.113 1763	0.482 443	1.276 1172	13	380.4±5.7	0.1(20)	80.2±7.4	13.47±0.18 (43)	1.16	>105 °C, 100–65 Ma (>110 °C, >75 Ma) 40–60 °C, 20–0 Ma

[a] All numerical values for stratigraphic ages assigned following [18].

[b] ρ_s=spontaneous track density. ρ_i=induced track density. ρ_D=glass dosimeter track density. Numbers in parentheses show the number of tracks counted in determining all track densities.

[c] Central age [19], used for samples containing a significant spread in single grain ages ($P(\chi^2)<5\%$), otherwise the pooled age is quoted. All ages were calculated using the zeta calibration approach of Hurford and Green [20], using the zeta values shown (CN5 glass). All errors quoted at ± 1σ. All analytical details are as described in [21], with the exception that some thermal neutron irradiations show a significant flux gradient, in which case the appropriate value of ρ_D was determined by linear interpolation through the stack of grain mounts.

[d] Numbers in parentheses show the number of track lengths measured.

[e] Thermal history interpretation of AFTA data is based on assumed heating and cooling rates of 1 °C/Ma and 10 °C/Ma, respectively. Quoted ranges for paleotemperature and onset of cooling correspond to±95% confidence limits. Where quoted maximum paleotemperatures represent a lower limit (e.g. >120 °C), the times quoted for the onset of cooling refer in these samples to the time at which the sample cooled through the quoted paleotemperature. Conditions shown in italics are tentatively required in order to provide an improved fit to the data but are not definitely required by the data.

Th)/He ages in apatite in geological conditions, which can be used to extract quantitative thermal history constraints typically in the temperature range 20–80 °C.

In sedimentary basins, the method has proven particularly useful when integrated with other paleo-thermal techniques such as apatite fission track analysis (AFTA®) and vitrinite reflectance, allowing complementary information over a wider range of paleotemperatures [e.g. 9,10]. However, while these initial studies showed a high degree of consistency between AFTA and the apatite (U–Th)/He system, an increasing body of evidence is now emerging which contradicts this apparently simple picture. Published He diffusion systematics [6] and fission track annealing systematics [11,12] predict that an apatite (U–Th)/He age should, in most conditions, be much younger than an apatite fission track age in the same sample. But an increasing number of recent studies are reporting apatite (U–Th)/He ages which are older than expected on the basis of apatite fission track data from the same region [e.g. 13,14,15,16]. In some cases, reported (U–Th)/He ages are even significantly older than the fission track ages measured on apatites from the same rock sample [e.g.15].

As discussed by Hendricks and Redfield [15], many other cases of such "anomalously old" (U–Th)/He ages (by comparison with fission track ages) have been informally reported and set aside as incompatible with the accepted sensitivities of the two techniques. Such examples are usually considered as reflecting problems with the (U–Th)/He system, although Hendricks and Redfield [15] recently suggested that the explanation lay in anomalous fission track annealing behaviour at low temperatures due to non-thermal processes.

Here we present data from a range of geological settings to document a systematic discrepancy between the two techniques, which becomes more pronounced in samples with older fission track ages (except for samples with very low uranium contents). Based on data from a well-controlled test case in which independent constraints are available on the underlying thermal history, we demonstrate that this progressive discrepancy arises not from anomalous fission track annealing behaviour but as a result of a change in the He retention properties of apatite, which appears to be linked to the degree of accumulated radiation damage within the crystal lattice.

2. Methodology

Our strategy in this study is to test the consistency between AFTA and apatite (U–Th)/He dating in a wide variety of different settings. In order to achieve this, we adopt as a starting position the view that AFTA provides a reliable assessment of the thermal history of the apatite sample, and use this as a basis for assessing the (U–Th)/He results. The methodology employed has been described in detail elsewhere [9,10], and is not repeated here. AFTA is initially used to define the range of thermal history solutions that are consistent with the measured fission track parameters in each sample (within 95% confidence limits). Modelling the variation of (U–Th)/He ages with radius [6] expected from various thermal histories within the range of acceptable solutions defined from AFTA, and comparing the results with measured (U–Th)/He ages, then allows us to test whether the measured apatite (U–Th)/He ages are consistent with the results from AFTA. If so, further modelling allows definition of a narrower range of viable thermal histories which are consistent with both datasets. Alternatively, if the measured (U–Th)/He ages are not compatible with the predictions based on the thermal history derived from AFTA, then either the AFTA or the (U–Th)/He data (or possibly both) do not conform to the systematics used in the interpretation process. Analysis of a number of samples from different geological environments allows investigation of the degree of mismatch as a function of key variables.

All practical aspects of AFTA for this study, including data gathering, analysis and thermal history interpretation, are as described in detail elsewhere [9,10]. Summary AFTA parameters from all analyses discussed here are presented in Table 1, together with the resulting thermal history solutions. Note that in the approach to thermal history interpretation of AFTA data employed in this study, we adopt an episodic thermal history framework, consisting of a series of heating and cooling intervals. We do not attempt to constrain the entire thermal history, but concentrate on those aspects of the history that dominate the data, i.e. maximum or peak paleotemperatures and the time at which the sample began to cool from those paleotemperatures. AFTA data are largely insensitive to other parts of the history (see [17] for more details of this aspect of the technique). This approach is contrary to conventional thermochronological practice, in which monotonic cooling histories are the norm. We believe that the episodic style is more realistic, even in the basement terrains included in this study (see later discussion of results from specific regions).

Most aspects of the (U–Th)/He analyses were as described by Crowhurst et al. [9], except that gas extraction was performed using a Nd-YAG laser system at ~1 to 2 W of power applied to the sample for ~10 min, heating the sample to a temperature of ~1000 °C. With the lower blanks afforded by the laser-based system (compared to the more traditional furnace-based system), single grains

can be analysed, although in some cases multiple grains are combined in a single run. In most samples, at least five individual grains of apatite were analysed, with most analyses carried out at the CSIRO Low Temperature Thermochronology Facility in Perth, Western Australia, while in some case replicates were also carried out at Caltech. Careful grain selection ensured that analysed grains were free of inclusions that may contain U and Th and thus produce spurious results. A small number of analyses also included determination of Sm, to check the contribution of He from the decay of ^{147}Sm (analyses performed at the University of Melbourne). Results for each sample discussed here are summarised in Table 2 (note that analyses from different laboratories were reported in variable formats, so not all information is available for all analyses).

Details of the approach to modelling of (U–Th)/He ages adopted in this study are also as discussed at length elsewhere [9,10], except that in-house software was used. This largely replicates the methods in [6], but models the influence of helium diffusion and alpha particle ejection simultaneously, following the suggestion of Meesters and Dunai [22]. Note however that the small influence of this factor (up to ~20% [22]) is not sufficient to influence any of the conclusions reached in this study. We follow the customary practice of assuming that He diffusion in all apatites conforms to the systematics defined in the Durango apatite [6]. Testing of this assumption can be considered as one of the aims of this study.

3. West Greenland

Apatite fission track ages in four samples (GC861-2, -3,-4 and -5) of Precambrian basement from a coastal elevation section north of Sisimut in West Greenland (Table 1) show little change between sea level and an elevation of 750 m (Fig. 1), with all ages falling consistently in the range 180 to 260 Ma, with typical two-sigma errors of 20 to 40 Ma (Table 1). These samples are located to the east of a major Cretaceous rift located offshore along the coast [23] and the fission track ages are interpreted as representing Mesozoic–Cenozoic cooling associated with the initial stages in the formation of the present-day continental margin of West Greenland [24]. The slightly higher measured age in sample GC861-3 reflects a higher Cl content in apatites from this sample.

Measured (U–Th)/He ages in individual apatite grains from an initial study of these samples (Table 2, Fig. 1) show varying degrees of consistency. Ages in five grains from the highest elevation sample are highly consistent, but the degree of scatter in the ages within each sample generally increases downwards through the section, with some grains in the samples from close to sea level giving (U–Th)/He ages which are much older than the majority. The dominant age grouping within each sample decreases only slowly with decreasing elevation, in similar fashion to the fission track ages. Note that as with all other samples analysed for this study, these grains were checked very carefully prior to analysis to ensure the absence of uranium/thorium-rich inclusions, following the procedures outlined in [9], so the scatter in ages cannot be explained by this factor. In addition, none of the analyses reported in this study showed significant “re-extracts” (as discussed in [9]). While the source of this scatter in individual grain He ages is not known, it is not the prime focus of this study and detailed investigation of the underlying causes of such scatter will be dealt with elsewhere,

Track length data in these samples show that they did not cool rapidly to near-surface temperatures (Table 1). Based on the accepted systematics of both techniques, we would therefore expect the He age to be lower than the FT age in each sample, reflecting the different thermal sensitivities of the two techniques. Instead, in most samples the individual grain (U–Th)/He ages are generally close to or older than the fission track age (Fig. 1).

Given the higher degree of reproducibility of the individual (U–Th)/He ages in the highest elevation sample, GC861-2, compared to the other samples, we focus further discussion on this sample (while similar comments apply to all samples). Fig. 2 illustrates the thermal history solution extracted from the AFTA data in this sample, and the fit of the solution to the measured parameters. This solution is consistent with all other data from the region, and forms part of a coherent thermal history framework [24], so there is no apparent reason to doubt the validity of this thermal history. AFTA suggests that the sample cooled from between 100 and 110 °C some time between 240 and 185 Ma, then cooled from a subsequent peak paleotemperature in the range 75 to 105 °C beginning some time between 190 and 80 Ma and finally cooled from between 40 and 75 °C beginning some time between 90 and 15 Ma. Each of these cooling episodes are interpreted as representing regional cooling episodes beginning in the intervals 230–220 Ma, 160–150 Ma and 36–30 Ma as defined from a larger dataset [24].

Based on the best-fit thermal history solution derived from AFTA in sample GC861-2 (Fig. 2), the predicted variation of (U–Th)/He age with grain radius is also shown in Fig. 2, where it is compared with measured (U–Th)/He ages in this sample from Fig. 1 and also

Table 2
Apatite (U–Th)/He dating results

Sample number	^{4}He (ncc)	Total U (atoms × 10^{12})	U (ppm)	Total Th (atoms × 10^{11})	Th (ppm)	Total Sm (atoms × 10^{12})	Sm (ppm)	Grain radius (μm)	F_T[a]	Uncorrected (U–Th)/He age (Ma)	Corrected (U–Th)/He age (Ma)
West Greenland											
GC861-2a	6.899±0.003	0.815±0.034	43	1.361±0.063	7	–	–	65	0.79	198.2	212.9±6.6
GC861-2b	19.74±0.004	1.875±0.075	66	3.810±0.164	13	–	–	75	0.81	206.7	255.2±8.1
GC861-2c	3.484±0.003	0.382±0.016	18	0.466±0.021	2	–	–	75	0.79	182.7	231.2±7.3
GC861-2d	13.19±0.004	1.441±0.060	44	5.653±0.242	17	–	–	80	0.83	173.1	208.6±6.5
GC861-2e	9.684±0.004	1.007±0.041	28	3.619±0.157	10	–	–	80	0.82	183.0	223.1±6.9
861-2g	29.776±0.070	3.31±0.14	48	2.45±0.10	3	–	–	105	0.86	182.1	211.8±7.2
861-2h	24.823±0.038	3.05±0.13	46	2.90±0.12	4	–	–	102.5	0.86	164.5	191.3±6.5
861-2I	34.325±0.006	3.17±0.13	60	3.12±0.14	6	–	–	85	0.83	217.5	262.0±8.5
861-2j	19.311±0.003	2.04±0.08	32	3.30±0.14	5	–	–	105	0.86	187.9	218.5±7.3
861-2k	19.099±0.006	2.06±0.08	53	3.54±0.16	9	–	–	80	0.82	184.1	224.4±7.1
861-2(a)	15.9 nmol/g		11		23			57	0.76	180.0	235.4
861-2(b)	60.3 nmol/g		57		26			57	0.76	172.0	224.0
GC861-2m	12.61		43		8		325		0.80	158.7	198.4±8.2
GC861-2n	7.12		42		6		310		0.80	144.5	180.6±7.0
GC861-3a	16.777±0.004	1.878±0.078	41.77	10.36±0.44	22.29			90	0.84	163.6	194.8±6.0
GC861-3b	1.961±0.003	0.140±0.006	3.26	3.116±0.140	7.02			90	0.84	191.2	227.6±6.2
GC861-3c	0.752±0.003	0.081±0.004	2.00	1.378±0.060	3.30			80	0.84	138.5	164.8±4.7
GC861-3d	6.72±0.003	0.265±0.014	8.12	7.619±0.337	22.58			75	0.82	312.1	380.6±9.7
GC861-3e	1.267±0.002	0.110±0.005	4.11	2.642±0.116	9.51			75	0.81	153.1	189.1±4.8
GC861-4a	17.928±0.013	1.97±0.25	61	5.02±0.63	15			80	0.82	177.3	216.2±24.9
GC861-4e	18.488±0.016	1.45±0.18	39.83	2.57±0.32	6.84			85	0.83	250.4	301.7±35.6
GC861-4f	7.723±0.008	0.384±0.048	19.37	1.36±0.17	6.62			70	0.80	375.3	469.1±54.1
GC861-4g	15.953±0.004	2.23±0.28	99.74	13.2±0.2	57.20			70	0.80	130.4	163.0±17.6
GC861-4h	29.928±0.004	3.27±0.41	131.37	14.6±0.18	56.75			70	0.80	171.4	214.1±23.8
GC861-5a	8.644±0.007	0.93±0.12	13.84	0.107±0.016	0.15			110	0.87	190.4	218.8±±26.7
GC861-5b	8.414±0.004	0.71±0.09	19.94	0.357±0.045	0.97			80	0.83	239.5	288.5±34.9
GC861-5c	7.260±0.005	1.16±0.15	26.62	0.218±0.028	0.48			85	0.83	128.6	155.0±18.7

Table 2 (*continued*)

Sample number	^{4}He (ncc)	Total U (atoms × 10^{12})	U (ppm)	Total Th (atoms × 10^{11})	Th (ppm)	Total Sm (atoms × 10^{12})	Sm (ppm)	Grain radius (μm)	F_T[a]	Uncorrected (U–Th)/He age (Ma)	Corrected (U–Th)/He age (Ma)
Yilgarn Block, Western Australia											
RD8-39a	0.486±0.012	0.048±0.021	13	0.232±0.012	6			35	0.64	187.68	293.3±8.7
RD8-39b	1.770±0.045	0.166±0.069	47	1.020±0.047	28			30	0.58	192.00	331.0±8.5
RD8-39c	1.398±0.035	0.114±0.047	27	0.442±0.021	10			37.5	0.66	231.51	350.8±10.5
RD8-39d	2.195±0.055	0.186±0.076	39	0.793±0.035	16.1			40	0.67	220.81	329.6±9.9
RD8-39e	1.479±0.037	0.136±0.056	26	0.659±0.031	12.1			40	0.64	201.39	314.7±9.0
RD8-39f	1.966±0.049	0.173±0.072	43	0.913±0.042	22.0			35	0.65	208.80	321.2±9.3
RD8-39g	2.392±0.060	0.209±0.086	52	1.150±0.052	27.6			37.5	0.65	208.87	321.3±9.3
RD8-39h	0.796±0.020	0.083±0.034	19	0.550±0.026	12.5			40	0.66	171.68	260.1±7.5
RD8-39i	0.508±0.015	0.062±0.026	25	0.325±0.015	12.5			35	0.57	151.59	266.0±7.2
RD8-39j	1.532		28.6		17.3		313.8	33	0.62	219.6	354.1±25.4
Cerberean Cauldron, Victoria											
8424-8a	30.103±0.004	4.33±0.18	139	0.953±0.054	3.0			77.5	0.82	240.71	293.6±9.7
8424-8b	47.289±0.005	5.79±0.24	147	1.570±0.074	3.9			77.5	0.83	281.07	338.6±11.3
8424-8c	24.906±0.004	3.42±0.14	106	0.991±0.050	3.0			72.5	0.8	251.54	314.4±10.1
8424-8d	27.103±0.004	3.66±0.15	103	2.440±0.114	6.7			75	0.82	253.63	309.3±10.1
8424-8e	19.736±0.004	2.39±0.10	191	0.802±0.037	6.2			50	0.72	283.38	393.6±11.4
8424-8 (a)	199.3 nmol/g		146.1		3.4			54.3	0.74	242.88	323.8
8424-8 (b)	206.3 nmol/g		149.7		4.3			51.4	0.74	245.14	329.4
8424-8 (c)	381.7 nmol/g		257.0		10.1			51.4	0.74	262.14	349.7
8424-8 (d)	195.1 nmol/g		167.2		3.2			45.7	0.72	208.90	289.2
8424-8 (e)	204.0 nmol/g		135.1		2.1			62.9	0.78	268.54	339.6
8424-8 (f)	229.9 nmol/g		167.5		3.3			45.7	0.71	244.63	342.6
8424-8f	15.695		165.8		8.7		404.0	40	0.70	234.2	334.6±22
8424-8g	24.152		209.9		4.1		490.5	45	0.71	229.7	323.5±21
8424-8h	20.854		218.7		4.4		458.3	50	0.72	253.2	351.6±24
8424-8j	8.688		152.2		4.6		362.2	38	0.68	216.7	318.7±21
Strangways Ranges, Northern Territory											
AP1a	1.366±0.004	0.055±0.003		3.34±0.15					1	213.54	213.5±7.1
AP1b	0.983±0.003	0.036±0.002		2.00±0.09					1	245.46	245.5±8.2

(continued on next page)

Table 2 (*continued*)

Sample number	^{4}He (ncc)	Total U (atoms × 10^{12})	U (ppm)	Total Th (atoms × 10^{11})	Th (ppm)	Total Sm (atoms × 10^{12})	Sm (ppm)	Grain radius (μm)	F_T[a]	Uncorrected (U–Th)/He age (Ma)	Corrected (U–Th)/He age (Ma)
Strangways Ranges, Northern Territory (continued)											
AP1c	0.51±0.003	0.020±0.001		0.99±0.05					1	246.60	246.6±8.3
AP1d	0.989±0.003	0.035±0.002		2.07±0.09					1	247.96	247.9±8.1
AP1e	1.313±0.003	0.052±0.002		2.96±0.14					1	225.07	225.1±7.4
AP1f	1.027±0.002	0.037±0.002		2.06±0.09					1	249.21	249.2±7.6
AP1g	0.569±0.002	0.019±0.001		1.19±0.05					1	253.25	253.3±8.3
AP1h	0.881±0.001	0.028±0.001		1.67±0.07					1	274.87	274.9±8.6
AP1i	0.859±0.001	0.033±0.001		1.81±0.09					1	238.92	238.9±8.1
AP1j	1.622±0.001	0.052±0.002		3.26±0.14					1	262.64	262.6±8.2
AP-1k	1.047	0.0170 ng		0.0967 ng		0.5529 ng		–	1	210.2	210.2±8.9
AP-1l	0.328	0.0050 ng		0.0304 ng		0.1541 ng		–	1	215.7	215.7±9.4
AP-1m	0.39	0.0067 ng		0.0344 ng		0.2009 ng		–	1	210.4	210.4±8.9
AP-1n	0.779	0.0123 ng		0.0697 ng		0.3640 ng		–	1	216.9	216.9±9.5
AP-1o	1.054	0.0162 ng		0.0950 ng		0.4733 ng		–	1	218.6	218.6±9.6
Snowdon, *North Wales*											
RD35-23a	0.327±0.001	0.040±0.002	2.9	2.09±0.09	14.6				0.76	77.0	101.2±2.4
RD35-23b	0.58±0.001	0.059±0.002	4.5	2.45±0.11	18.2				0.76	104.3	137.2±3.1
RD35-23c	0.432±0.001	0.051±0.002	4.7	2.56±0.11	23.0				0.74	81.9	110.7±2.5
RD35-23d	0.463±0.001	0.043±0.002	2.5	2.72±0.12	15.6				0.73	91.6	125.4±2.9
RD35-23e	0.255±0.001	0.026±0.001	1.0	1.80±0.08	6.4				0.7	78.6	112.2±2.5
Otway Basin, *Victoria*											
RD14-339a	0.711±0.018	0.161±0.089	2.9	11.12±0.53	19.6			90	0.84	35.41	42.2±1.6
RD14-339b	0.64±0.016	0.109±0.059	3.2	8.11±0.38	23.1			80	0.81	45.15	55.7±2.0
RD14-339c	0.575±0.015	0.109±0.059	2.9	8.05±0.38	21.1			90	0.84	40.77	48.5±1.8
RD14-339d	0.371±0.010	0.034±0.019	1.3	2.47±0.12	9.0			65	0.8	84.75	105.9±3.7
RD14-339e	0.36±0.009	0.198±0.111	7.7	11.0±0.51	41.4			75	0.81	16.68	20.6±0.7
RD14-339f	0.24±0.02	0.050±0.002	1.8	2.69±0.13	9.5			70	0.81	43.81	54.1±1.9
RD14-339g	0.80±0.02	0.184±0.008	7.2	5.68±0.25	21.4			75	0.80	53.26	66.6±2.1
RD14-339h	0.21±0.01	0.039±0.002	1.6	1.59±0.07	6.2			70	0.79	57.99	73.4±2.4
RD14-339i	0.54±0.01	0.077±0.003	3.6	3.25±0.14	14.2			75	0.80	74.24	92.8±2.9
RD14-339j	0.32±0.01	0.058±0.002	1.9	4.35±0.19	13.4			85	0.82	42.56	51.9±1.7

Table 2 (*continued*)

Sample number	^{4}He (ncc)	Total U (atoms × 10^{12})	U (ppm)	Total Th (atoms × 10^{11})	Th (ppm)	Total Sm (atoms × 10^{12})	Sm (ppm)	Grain radius (μm)	F_T[a]	Uncorrected (U–Th)/He age (Ma)	Corrected (U–Th)/He age (Ma)
Otway Basin, Victoria											
RD14-339n	0.113±0.004	0.031±0.015	6.0	1.800±0.080	34.8			45	0.70	32.20	46.00
RD14-339m	0.128±0.004	0.024±0.012	4.1	1.200±0.054	19.0			42.5	0.69	51.42	74.52
RD14-339o	0.051±0.003	0.026±0.011	5.2	1.680±0.075	32.5			35	0.66	16.46	24.94
RD14-339p	1.982±0.050	0.410±0.017	74.2	8.350±0.405	146.4			35	0.66	68.57	103.90
RD14-339k	0.168±0.005	0.049±0.020	4.4	1.460±0.066	14.1			55	0.75	42.60	56.80
RD14-339l	0.278±0.008	0.077±0.032	10.0	3.990±0.189	51.0			45	0.71	34.37	48.41
RD14-341a	0.993±0.025	0.185±0.010	33.6	4.19±0.20	73.3			45	0.67	73.32	109.4±3.4
RD14-341b	0.560±0.014	0.097±0.005	19.3	2.12±0.10	40.8			42.5	0.66	80.03	121.3±3.7
RD14-341c	0.883±0.022	0.012±0.006	20.9	3.17±0.15	55.5			42.5	0.69	97.23	140.9±4.4
RD14-341d	1.162±0.029	0.012±0.006	10.5	3.52±0.17	30.2			75	0.74	120.44	162.8±5.4
RD14-341e	0.371±0.010	0.060±0.003	14.9	1.59±0.08	38.2			42.5	0.64	80.16	125.3±3.7
RD14-341f	0.42±0.01	0.062±0.003	17.6	1.66±0.08	45.6			37.5	0.64	86.78	135.6±3.5
RD14-341g	0.22±0.01	0.049±0.002	12.3	0.378±0.021	9.1			40	0.66	77.02	116.7±3.6
RD14-341h	0.35±0.01	0.086±0.004	28.5	1.74±0.09	55.8			32.5	0.58	57.24	98.7±2.4
RD14-341i	0.41±0.01	0.093±0.004	30.9	1.80±0.09	57.7			32.5	0.56	63.63	113.6±2.6
RD14-341j	0.53±0.01	0.080±0.003	12.7	2.24±0.11	34.5			35	0.65	83.85	129.0±3.5

[a] F_T: Size correction factor [45].

from a number of additional analyses undertaken in Perth and in Caltech to check the reproducibility of the ages from this sample (Table 1). Almost all of the individual grain ages are reproducible within analytical errors, including results from different laboratories.

Despite this generally excellent reproducibility, all of the measured (U–Th)/He ages are much older than those predicted from the AFTA-based thermal history solution. Also shown in Fig. 2 are the predicted He age vs radius trends for various thermal history conditions within the range of conditions allowed by the AFTA data in the most recent paleo-thermal episode. It is clear that none of these conditions provides predictions that approach the measured ages, and even leaving out this episode completely results in predicted ages slightly less than 150 Ma for all radii, still much younger than the measured ages. These predicted ages are dominated by the second of the three paleo-thermal episodes identified from the AFTA data, in which the sample cooled from 90 °C at 150 Ma in the best-fit solution.

It is clear from Fig. 2 that only by moving this cooling episode back to around 200 Ma or earlier will predicted (U–Th)/He ages match the measured values. But such a scenario would result in an older fission track age and a track length distribution dominated by long tracks with lengths around 14 μm, which does not match the measured AFTA data. Thus, we conclude that the two datasets cannot be explained within a consistent thermal history framework. In fact, this is evident simply from the fact that most of the measured (U–Th)/He ages are older than the fission track age, which precludes a consistent explanation based on accepted systematics for the two methods.

One possible reason why (U–Th)/He ages might be anomalously old could be a significant contribution to the He budget in these grains from alpha decay of

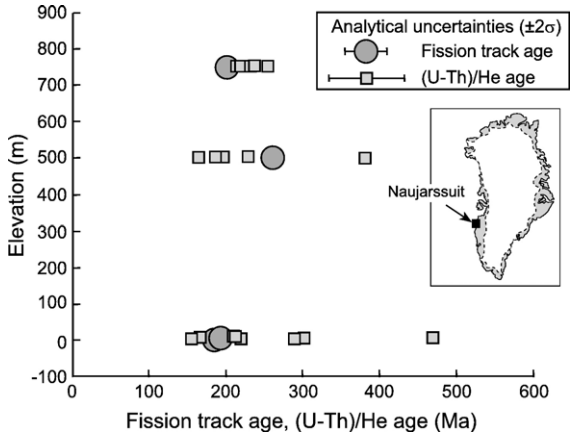

Fig. 1. Apatite fission track and (U–Th)/He ages in four samples from West Greenland, from Tables 1 and 2, plotted against sample elevation.

^{147}Sm, usually assumed to be negligible in routine (U–Th)/He dating, but shown to be significant in some cases [e.g. 25]. For this reason, (U–Th–Sm)/He ages were determined in two grains, with the explicit inclusion of Sm analyses. As shown in Table 2 and Fig. 3, these ages are towards the younger end of the range of He ages, suggesting that any contribution of He from ^{147}Sm alpha decay in these grains is clearly only of minor significance, and this cannot explain the discrepancy between the two techniques.

4. Yilgarn granite

Sample RD8-39 was collected from an outcrop of crystalline basement at Northam, north east of Perth, Western Australia, forming part of the Yilgarn Craton. A recent apatite fission track study [26] revealed a history of major Phanerozoic erosion and exhumation of the Yilgarn Craton, contradicting long-held views regarding the stability of the region. Combining these results with studies of detrital zircons in sedimentary basins adjacent to the craton [27] suggest that much of the eroded section consisted of an Early Paleozoic sedimentary cover, which supports the episodic style of thermal history interpretation involving repeated cycles of heating (burial) and cooling (exhumation) that we have investigated in this sample.

AFTA data from this sample are summarised in Table 1. The variation of fission track age with wt.% Cl and the track length distribution (all apatites contain between 0.0 and 0.1 wt.% Cl) measured in sample RD8-39 are illustrated in Fig. 3, together with the best-fit thermal history and the AFTA parameters predicted from this history. The best-fit thermal history contains three cooling episodes, involving cooling from 100 °C or above some time in the interval 500 to 380 Ma, followed by cooling from a peak paleotemperature between 65 and 75 °C which began between 240 and 100 Ma, and a later cooling episode from a poorly defined peak value less than 75 °C during the last 100 Myr. This history provides a good fit to the measured AFTA data (Fig. 3), and is consistent with Early Paleozoic erosion followed by deposition of a Paleozoic and Mesozoic cover prior to the onset of exhumation during the Late Mesozoic, matching the suggested evolution in previous studies [26,27].

Measured (U–Th)/He ages in ten individual apatite grains from this sample (Table 2) are also plotted against grain radius in Fig. 3. The ages show a rather higher degree of scatter than suggested by the analytical uncertainties, but overall define a consistent group of values between 250 and 350 Ma which are younger than the fission track age (also plotted with the He ages in Fig. 3). Thus, at first sight, the two techniques fall in the appropriate temporal relationship.

However, the variation of (U–Th)/He age with grain radius predicted from the best-fit AFTA thermal history using the Durango apatite diffusion systematics from [6] falls well below the measured (U–Th)/He ages in Fig. 3, echoing the experience with the West Greenland samples discussed earlier. Also shown in Fig. 3 are predicted (U–Th)/He age vs radius trends for a number of variations on the best-fit AFTA history, where the track length distributions and variation of fission track age with wt.% Cl predicted from these histories are also shown. In order to match the measured (U–Th)/He ages it is necessary to decrease the peak Mesozoic paleotemperature to around 50 °C or less, but this results in a pronounced mismatch between observed and predicted AFTA parameters, particularly in terms of the track length distribution which becomes dominated by much longer lengths compared to the measured distribution. The predicted FT age is less sensitive to these changes because this is dominated by the earliest cooling episode.

Thus, the measured (U–Th)/He ages are much older than expected on the basis of the AFTA data in this sample, and it is not possible to define a thermal history that is consistent with both techniques. Note that a (U–Th–Sm)/He age was measured in one grain from this sample (Table 2), the results of which agree with the older (U–Th)/He ages, suggesting that the contribution from ^{144}Sm to the He budget of this sample is not significant.

5. Lake Mountain Rhyodacite

The Lake Mountain Rhyodacite is the uppermost unit preserved in the volcanic fill of the Cerberean cauldron

in central Victoria, Australia, one of several sub-volcanic calderas of Upper Devonian age in the region. Apatites and zircons from this unit were investigated as a potential age standard for fission track dating by Green [28], who reported a mean crystallization age of 368±3 Ma based on published K/Ar and Rb/Sr ages. More recently, Compston [29] reported a SHRIMP zircon U/Pb age of 375±1 Ma. In the adjacent Mount Howitt Province, volcanic units of similar age are overlain by Devonian–Carboniferous red-beds [30], and a similar former cover seems likely for the Lake Mountain Rhyodacite.

AFTA parameters from a sample of Lake Mountain Rhyodacite, together with the resulting thermal history interpretation, are summarised in Table 1 and illustrated in Fig. 4. A particular feature of these apatites is the very high uranium content of 74 ppm, and the associated very high spontaneous track densities around 10^7 tracks/cm^2. Such track densities, combined with the relatively long mean track length of 13.2 μm, make accurate track counting difficult, due to track overlap. In fact, the majority of grains in the sample contain spontaneous track densities which are so high that individual tracks cannot be resolved and the grains are uncountable. This is reflected in the higher mean uranium content of 164 ppm in grains analysed by (U–Th)/He dating (Table 2), which are not selected on the basis of U content.

The thermal history extracted from the AFTA data (Fig. 4) contains two episodes of cooling; an earlier episode in which the sample cooled from >100 °C some time between 320 and 270 Ma, and a later episode involving cooling from a peak paleotemperature between 50 and 70 °C beginning some time between 120 and 0 Ma. The earlier episode is interpreted as representing burial below a Late Devonian to Carboniferous sedimentary sequence (see above) and subsequent uplift and erosion during Late Carboniferous to Permian times. The later episode may represent the effects of Cretaceous cooling of relatively minor magnitude similar to that seen in many apatite fission track studies across SE Australia (e.g. [31]), or alternatively could represent Late Miocene exhumation similar to that identified from AFTA in the sediments of the Otway Basin [10].

Measured He ages from three laboratories are listed in Table 2 and are also plotted against grain radius in

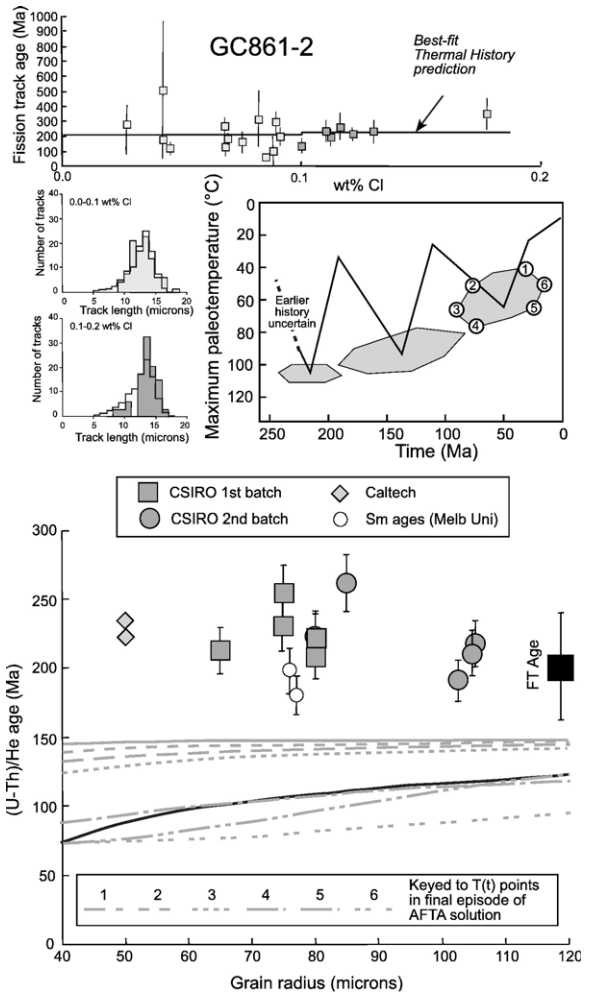

Fig. 2. Upper: AFTA data in West Greenland sample GC861-2 (summary parameters provided in Table 1) and the associated thermal history interpretation. Measured track length distributions are shaded; distributions predicted from the best-fit history in two compositional groups are unfilled. In this and other figures, the trend of fission track age with wt.% Cl predicted from the best-fit history is shown as a solid black line. AFTA data define three episodes of cooling, with the range of acceptable values (95% confidence limits) of maximum/peak paleotemperature and the time at which cooling began from that paleotemperature being shown by the shaded polygons. The pattern of variation of fission track age with wt.% Cl and the track length distributions in two compositional groups predicted from the best-fit thermal history are compared with measured data, demonstrating the good fit. Points 1 to 6 in the most recent paleo-thermal episode are used as the basis for modelling He ages in the lower plot as the earlier episodes involve paleotemperatures at which no He should be retained according to the He diffusion systematics in [6]. Lower: (U–Th)/He ages in individual apatite grains from West Greenland sample GC861-2, plotted against grain radius (from Table 2). The fission track age is also plotted as the large black square. The age vs radius trends predicted from the best-fit thermal history solution derived from AFTA (using published He diffusion systematics [6]) is shown as the solid black curve, while trends labelled 1 to 6 refer to different maximum temperatures in the most recent episode allowed by AFTA (Fig. 2). The solid grey curve shows the trend predicted after omitting the later event completely. None of the predicted trends approach the measured ages, which are thus anomalously old compared to the AFTA data.

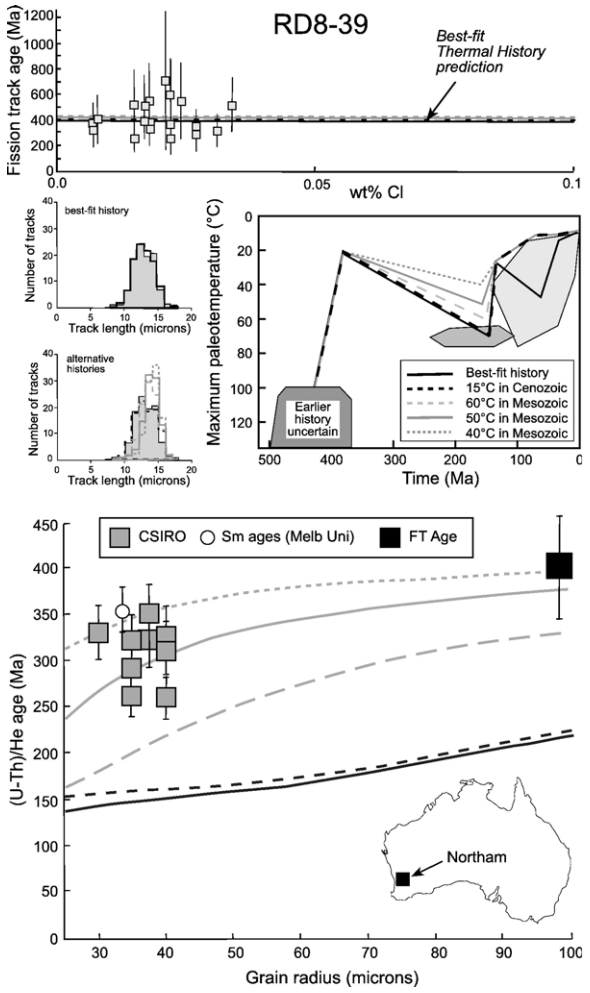

Fig. 3. Upper: AFTA data in Yilgarn Block sample RD8-39 (summary parameters provided in Table 1) and the associated thermal history interpretation. The measured track length distribution is shaded; distributions predicted from various thermal histories are unfilled, with line type keyed to different thermal histories. AFTA data define three episodes of cooling, as shown (details as in Fig. 2). Various alternative thermal history solutions (outside the range of solutions allowed by AFTA) used in modelling He ages in Fig. 5 are also illustrated, and the variation of fission track age with wt.% Cl and the length distributions predicted from these histories are compared with the measured ages (top) and length distributions (lower left). Lower: (U–Th)/He ages in individual apatite grains from Yilgarn Block sample RD8-39, plotted against grain radius (from Table 2). The fission track age is also plotted as the large the black square. The age vs radius trends predicted from the best-fit thermal history solution derived from AFTA (using published He diffusion systematics [6]) is shown as the solid black curve, while trends shown as dashed lines refer to alternative thermal histories outside the range of solutions defined from AFTA as shown in the upper Figure. To explain the measured (U–Th)/He ages in this sample, a peak Mesozoic paleotemperature around 50 °C or less is required, contrary to the range of 65 to 75 °C defined from AFTA. The measured (U–Th)/He ages are thus anomalously old compared to the AFTA data.

Fig. 4. Results from all three laboratories show a high level of consistency, but all of the ages are significantly older than the fission track age, which is also plotted with the He ages in Fig. 4. This immediately shows that these ages cannot be interpreted using the usual systematics, which demand that He ages should be lower than the fission track age. Note that the four ages determined at the University of Melbourne also incorporated analysis of ^{147}Sm, and again the similarity between these and the simple (U–Th)/He ages suggests that the contribution of helium from this source is not significant.

Also shown in Fig. 4 is the variation of (U–Th)/He age predicted from the best-fit AFTA solution, together with two other scenarios within the allowed range of solutions derived from the AFTA data, one involving cooling from 60 °C at 95 Ma (representing a mid-Cretaceous episode) and another in which the sample cooled from a peak of 50 °C at 10 Ma representing Late Miocene cooling. In both cases, the sample was cooled to 10 °C within 5 Myr after the onset of cooling, to maximise the possible (U–Th)/He age. The Late Miocene scenario represents a minimum post-Paleozoic heating scenario within the range allowed from AFTA. In all cases, predicted (U–Th)/He ages are much lower than the measured ages, as might be expected since the measured He ages are older than the FT age. Thus, the two datasets in this sample cannot be accommodated within a common thermal history framework using accepted systematics.

6. Mud tank apatite

Apatite megacrysts occur within the Mud Tank Carbonatite, in the Strangways Ranges of the Northern Territory NE of Alice Springs. A zircon U–Pb age of 732±5 Ma and a whole-rock Rb–Sr age of 735±75 Ma were reported by Black and Gulson [32], while younger Rb–Sr biotite ages between 319 and 349 Ma were interpreted as representing overprinting during the Alice Springs Orogeny [33].

AFTA parameters measured in apatite fragments from a large (several cm) apatite megacryst are summarised in Table 1 and illustrated in Fig. 5. The pooled fission track age of 298±23 Ma is just slightly younger than the biotite Rb–Sr ages (above), suggesting rapid post-orogenic cooling. The thermal history solution derived from the AFTA data (Fig. 5) confirms this, with cooling from >100 °C in the interval 380 to 270 Ma and from a later peak between 50 and 85 °C beginning some time between 280 and 90 Ma, after which the sample remained below 50 °C. The quite wide

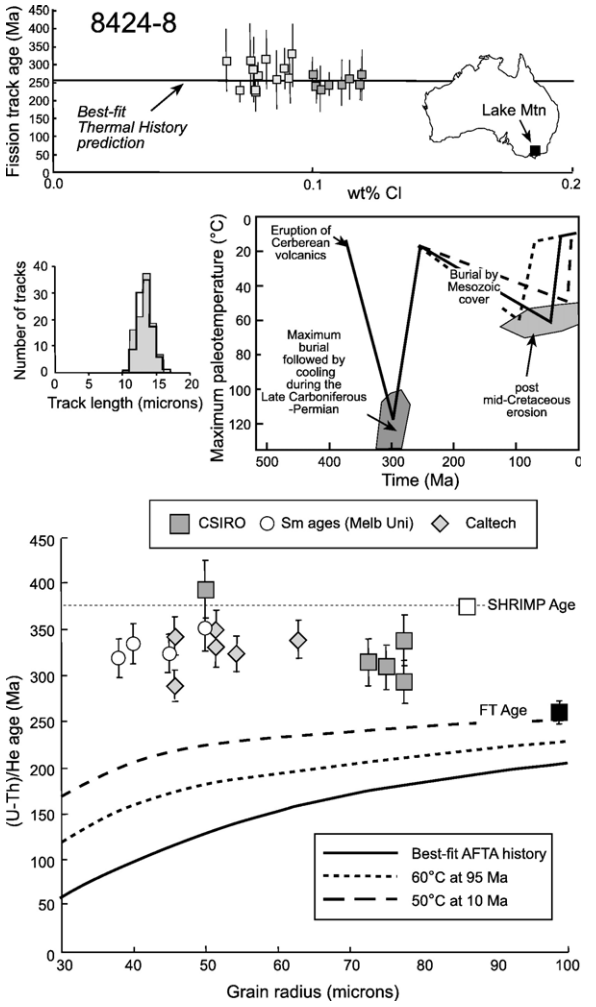

Fig. 4. Upper: AFTA data in Lake Mountain Rhyodacite sample 8424-8 (summary parameters provided in Table 1) and the associated thermal history interpretation. The measured track length distribution is shaded; the distribution predicted from the best-fit history is unfilled. AFTA data define two episodes of cooling, with 95% confidence regions for each episode shown by the shaded polygons. The variation of fission track age with wt.% Cl and the length distribution predicted from the best-fit history are compared with the measured ages (top) and length distributions (lower left). Lower: (U–Th)/He ages in individual apatite grains from Lake Mountain Rhyodacite sample 8424-8, plotted against grain radius (from Table 2). The fission track age and SHRIMP U–Pb age are also plotted as the large black and white squares, respectively. The age vs radius trend predicted from the best-fit thermal history solution derived from AFTA (using published He diffusion systematics [6]) is shown as the solid black curve, and significantly underestimates the measured ages. Trends of age vs radius predicted by two alternative thermal histories outside the range of solutions defined from AFTA are also shown. These histories also fail to explain the measured (U–Th)/He ages in this sample, which are thus anomalously old compared to the AFTA data.

range of timing for the later episode reflects the relatively low magnitude of this episode. A particular feature of the AFTA data in this apatite is the low uranium content of the analysed grains at only 3.2 ppm. This results in a quite large error in the pooled age, despite analysis of 20 large fragments. Nevertheless, the predicted parameters provide a good match to the data and the thermal history solution is considered reliable within the range of allowed uncertainty. This history is similar to those defined across Central Australia by Tingate et al. [34,35], representing progressive regional exhumation through Late Phanerozoic times.

Measured (U–Th)/He ages in ten individual fragments from a large (cm-sized) apatite megacryst are plotted in Fig. 5 where they are also contrasted with the fission track age. The He ages are highly consistent within analytical uncertainties, and all fall below the pooled fission track age. Five (U–Th–Sm)/He ages are also shown in this figure, and these also show a high degree of internal consistency, although they are all consistently less than the (U–Th)/He ages. The reason for this is not known at present, and we focus on the (U–Th)/He ages in the following, but recalculation of these ages without taking Sm into account shows that any contribution from ^{147}Sm decay to the He budget in this apatite is negligible [36]. The apparent systematic difference between these and the (U–Th)/He ages remains unexplained.

Because these He ages were determined on fragments produced by crushing a large megacryst, they are not expected to show significant variation with grain radius, but in Fig. 5 the variation of (U–Th)/He age with grain radius predicted from the best-fit thermal history solution from AFTA (also shown in Fig. 5) using the Farley (2000) He diffusion systematics is shown for comparison. The measured He ages lie on the projection of this trend towards larger radii, suggesting that they are consistent with the predicted values. Thus in this apatite, characterised by a notably low uranium content, the (U–Th)/He and fission track systems appear to show a response which is consistent with the expected systematics of each technique.

7. Snowdon

Sample RD35-23 was collected from an outcrop of a tuffaceous unit of the Ordovician Snowdon Volcanic group, from the west flank of Snowdon, North Wales. A pooled fission track age of 234 ± 14 Ma was determined from nineteen apatite grains from this sample (Table 1). Variation of individual grain ages with wt.% Cl and the distribution of confined track lengths measured in this sample are shown in Fig. 6, together with the resulting best-fit thermal history solution and the predicted AFTA parameters from this history. A series of paleo-thermal

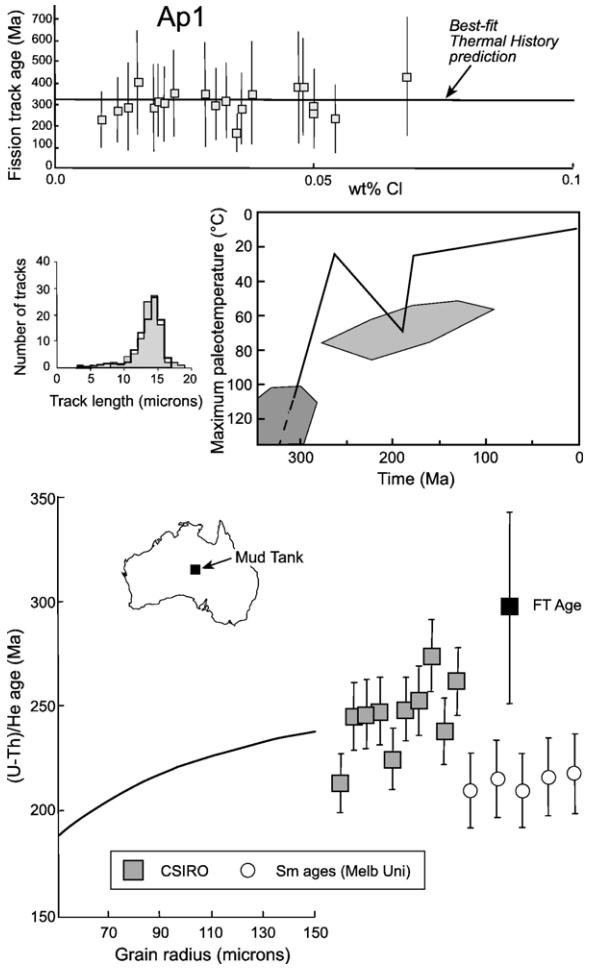

Fig. 5. Upper: AFTA data in Mud Tank apatite sample Ap1 (summary parameters provided in Table 1) and the associated thermal history interpretation The measured track length distribution is shaded; the distribution predicted from the best-fit history is unfilled. AFTA data define two episodes of cooling, as shown (with 95% confidence regions around best-fit values shown by the shaded polygons). The variation of fission track age with wt.% Cl and the length distribution predicted from the best-fit history are compared with the measured ages (top) and length distributions (lower left). Lower: (U–Th)/He ages in individual fragments of Mud Tank apatite Ap1 (from Table 2). Because these are fragments from a large (several cm) megacryst, ages are not plotted against grain radius but are simply plotted in order. The fission track age is also plotted as the large black square. The age vs radius trends predicted from the best-fit thermal history solution derived from AFTA (using published He diffusion systematics [6]) is shown as the solid black curve, and the projection of this trend approaches the measured ages, suggesting that the two systems show consistent response in this sample.

episodes are defined (Table 1). The earliest is interpreted as representing Variscan (end-Carboniferous) cooling, while the second episode represents a Triassic–Early Jurassic cooling episode which Holford et al. [37] interpreted as representing footwall uplift associated with normal fault-controlled subsidence in the adjacent Cardigan Bay Basin. The most recent episode shown in Fig. 6 overlaps two regional cooling episodes recognised across the region in the Early Cretaceous and Early Cenozoic [37], and may represent either of these, or possibly the unresolved effects of both. The uranium content of apatite from this sample is again quite low at 7 ppm (Table 1). In fact, most individual grains contain between 3 and 6 ppm, and the mean is increased by a small number of higher uranium grains. The significance of the low uranium content in apatites from this sample is discussed later.

(U–Th)/He ages measured in five grains of apatite from this sample are listed in Table 2 and plotted against grain radius in Fig. 6. The He ages show rather more scatter than suggested by the analytical uncertainties, but overall define a consistent grouping of ages around 100–140 Ma. The variation of (U–Th)/He age predicted from the best-fit AFTA history featuring a peak paleotemperature of 62 °C at 97 Ma (Fig. 6), also plotted in Fig. 6, falls just slightly higher than the measured ages, but changing the peak paleotemperature to 80 °C at 120 Ma, 70 °C at 100 Ma or 60 °C at 60 Ma results in predicted trends that span the range of measured ages (Fig. 6). Repeated modelling using various combinations of peak paleotemperature and onset of cooling allow definition of the range of conditions that provide predictions which match both the measured AFTA and (U–Th)/He ages (Fig. 6).

Thus, similar to the experience with the Mud Tank apatite, in apatites from the Snowdon Volcanic group the (U–Th)/He and fission track systems appear to show a response which is consistent with the expected systematics of each technique. These two apatites are both characterised by low uranium contents around 3 to 5 ppm, and as discussed below, we suggest this factor is significant in producing consistent data from both systems in these samples.

8. Synthesis

Discussion of AFTA and (U–Th)/He data in previous sections has shown that in some samples (e.g. West Greenland, Yilgarn Block, Lake Mountain) the two systems are widely disparate while in others (e.g. Mud Tank, Snowdon) the two systems provide apparently consistent indications of the underlying thermal history. A variety of factors have been suggested previously as potentially causing a disparity between the two systems, notably slow cooling [38] and zoning of Uranium and/or Thorium [22]. However, one clear distinguishing feature in this study between samples in which the two systems

give consistent results and those giving conflicting results is the uranium content of the apatite grains, with low values around 3 to 5 ppm in the two samples which provide consistent results, compared to much higher values (up to 100 ppm and above) in the other samples.

To investigate this further, Fig. 7 shows a plot of the ratio of the measured (U–Th)/He age to the value predicted from the best-fit thermal history derived from AFTA in the same sample, against the product of the measured FT age and the sum of the uranium content and 0.24 times the Th content (each in ppm), for all of the data listed in Table 2. This latter term is used because for timescales of 1 to 500 Myr, the production of He from thorium is roughly 0.24 times that from uranium. Also included in Fig. 7 are samples from the Fresne-1 well in the Taranaki Basin, New Zealand [9]. Note that these are based on analysis of multiple apatite grains, whereas the data from Table 2 are all based on single grains. Finally, a value for Durango apatite is also plotted in Fig. 7, reflecting the common observation that the fission track and He ages in this sample are equal.

Fig. 7 strikingly displays an obvious systematic relationship in which the discrepancy between the measured (U–Th)/He age and the value predicted from the history derived from AFTA increases progressively as the number of alpha decays over a time equal to the fission track age increases. Particularly significant in Fig. 7 is the concordancy of data from the Durango apatite, Mud Tank apatite and the apatite from Snowdon. In all these samples, measured He ages are close to the values predicted from the AFTA best-fit history and the function of U and Th is similar in all three samples. In contrast, predicted He ages in apatites from the West Greenland and Yilgarn samples are around twice the value predicted from the AFTA best-fit history, while corresponding values in apatites from the Lake Mountain Rhyodacite, characterised by the highest U contents, are around 2.5 times the values predicted on the basis of the AFTA history.

Note that use of the fission track age in the function of U and Th in Fig. 7 is simply a convenient measure to allow plotting of these results. In most cases the FT age does not actually represent the time over which tracks (or helium) have been retained, and is merely an

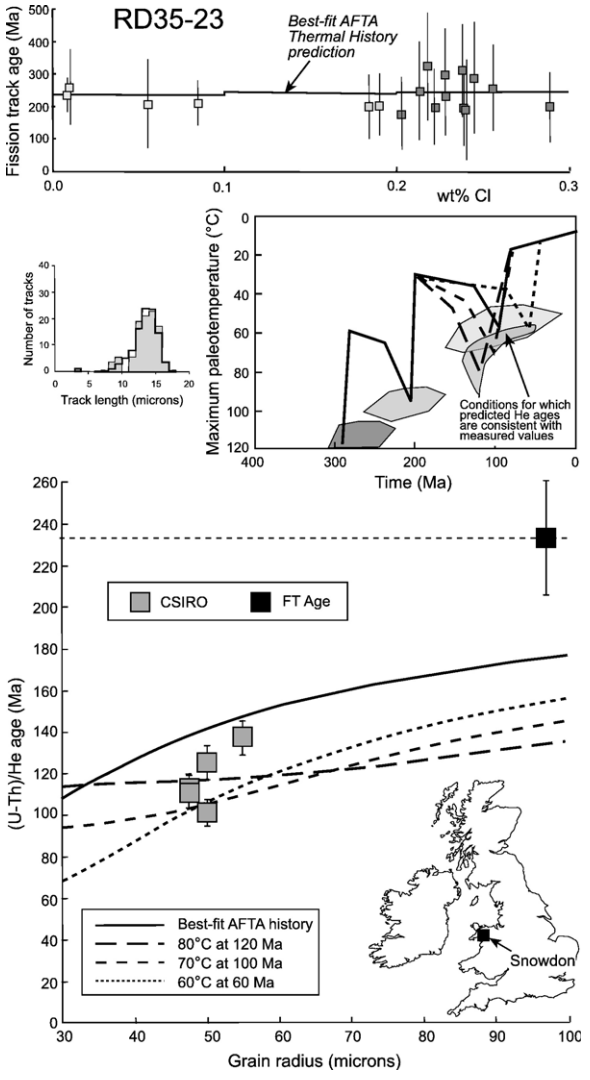

Fig. 6. Upper: AFTA data in Snowdon Volcanic group sample RD35-23 (summary parameters provided in Table 1) and the associated thermal history interpretation. The measured track length distribution is shaded; the distribution predicted from the best-fit history is unfilled. AFTA data define three episodes of cooling, with 95% confidence regions about the best-fit values shown by the shaded polygons. The variation of fission track age with wt.% Cl and the length distribution predicted from the best-fit history are compared with the measured ages (top) and length distributions (lower left). Alternative thermal histories used in modelling He ages for Fig. 11 are also shown. Comparison of modelled and measured He ages allows refinement of conditions during the most recent paleo-thermal episode which are consistent with both datasets (following [10]). Lower: (U–Th)/He ages in individual apatite grains from Snowdon Volcanic group sample RD35-23, plotted against grain radius (from Table 2). The age vs radius trend predicted from the best-fit thermal history solution derived from AFTA (using published He diffusion systematics [6]) is shown as the solid black curve, and slightly overestimates the measured ages. Trends of age vs radius predicted by two alternative thermal histories *within* the range of solutions defined from AFTA are also shown, and these are all consistent (in broad terms) with the measured (U–Th)/He ages in this sample. Continuing this process for more temperature–time combinations allows definition of the range of conditions during the most recent paleo-thermal episode which are consistent with both datasets (centre, right). Thus, the two systems show consistent response in this sample.

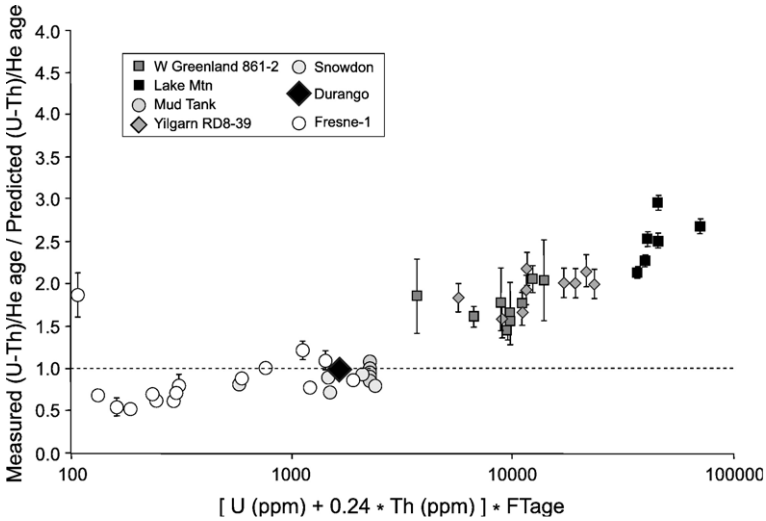

Fig. 7. The ratio of measured He age to the value predicted from the best-fit $T(t)$ solution derived from AFTA for each grain from each sample listed in Table 2 is plotted against the product of the measured fission track age (Table 1) and a function of uranium and thorium contents of each grain (Table 2) as shown. This term provides an approximate measure of the number of alpha particle decays from U and Th over a time equal to the measured fission track age. Data from the Fresne-1 well [9] are also included. If the behaviour of the two techniques conforms to the respective published systematics, the ratios should scatter around a value of 1. However, the results show a highly consistent departure from consistency, with measured ages becoming progressively higher than expected as the product of fission track age and U and Th contents increases.

expression of the underlying thermal history. Thus it is not immediately clear why Fig. 7 should show such a consistent relationship. Using the (U–Th)/He age instead of the fission track age results in a similar plot overall, but with more separation of the results at low values of (U+0.24*Th), and fission track age therefore appears to provide a better correlation, but the significance of this (if any) remains unclear.

Despite this uncertainty in interpreting the relationship, the consistency of these results clearly demonstrates that as the number of uranium and thorium decays increases (whether by alpha decay or fission), an increasing disparity emerges between the (U–Th)/He and AFT systems. Similar observations in Scandinavia have been interpreted [15,16] as due to "radiation-enhanced annealing" of fission tracks in apatite, such that in apatite samples with fission track ages around 400 Ma or above, tracks undergo greater degrees of annealing than expected from a purely thermal mechanism due to the large accumulated radiation dose. Such an explanation would provide a convenient explanation of the observations presented here. But an alternative interpretation is also possible, involving the modification of the helium retention properties of apatite, such that apatite becomes more retentive as the number of U and Th decays increases, suggesting a mechanism related to degree of radiation damage within the apatite lattice.

These two possible explanations have radical implications for the routine application of either AFTA or apatite (U–Th)/He dating, and confident use of either of these techniques demands that the origin of the inconsistency between the two techniques should be identified. The analyses discussed in the following section were undertaken with this in mind.

9. Analyses of a granite pebble and adjacent sediments from the Otway Basin

To resolve the origin of the increasing discrepancy between AFTA and (U–Th)/He dating as the number of U and Th decays increases, we applied both (U–Th)/He and AFTA to apatites from a ~10 cm diameter granite pebble (sample RD14-341) extracted from the Early Cretaceous volcanogenic sandstone of the Otway Group [39] from the shore platform at Kennett River, SE of Lorne in the Otway Basin, SE Australia, as well as apatites from the immediately adjacent sandstone sample (RD14-339). These two samples have shared a common history since deposition of the sediments in the Early Cretaceous, and thus results from the two techniques should reflect that common history. The higher uranium content of the granitic apatites, compared to the volcanogenic apatites, provides a direct comparison of the response of apatites containing different levels of accumulated radiation damage. In addition, the availability of vitrinite

reflectance data from coaly particles within the same sedimentary units provides an independent check on the thermal history of the samples. The utility of combining VR data with AFTA and (U–Th)/He data has been demonstrated in earlier studies (e.g. [9,10]).

The Otway Basin was formed during the early stages of rifting on Australia's southern margin, and contains a thick sequence of volcanogenic sediments of Early Cretaceous age. These sediments have been extensively studied by thermochronological techniques, and a consistent geological framework has emerged [10,40,41] involving a mid-Cretaceous paleo-thermal maximum due to a combination of elevated heat flow and deeper burial, from which cooling began at around 95 Ma. Subsequent burial in a lower heat flow regime led to a Late Miocene paleo-thermal peak, from which cooling began at ~10 Ma due to a regional Late Miocene episode of exhumation [10]. At various locations along the Otway coastline, granite pebbles occur within the sedimentary sequence. These were most likely derived from erosion of the basin margins, where Early Paleozoic granites (similar to those which now outcrop on King Island, Bass Strait) were uplifted and eroded during the mid-Cretaceous [42] as the volcanogenic sediments were deposited.

The presence of coaly material as individual plant fragments within the Otway Group sediments provides an important overall constraint on the post-depositional history of the apatites analysed from this location. A mean VR value of 0.71% was determined from 30 fields (analyst: Alan Cook), with a tight distribution of measured values providing a very high quality determination which is highly consistent with regional trends [10,40,41]. Using the methodology in [10], this corresponds to a maximum paleotemperature of 116 °C, which provides an independent constraint on the thermal history of the granite pebble and enclosing sandstone.

AFTA data in samples RD14-339 and-341, together with the resulting thermal history interpretations, are summarised in Table 1 and illustrated in Fig. 8, where the variation of FT age with wt.% Cl and the track length distribution predicted from the best-fit thermal history solution are also shown. The measured fission track age in apatite from the granite pebble (RD14-341) is 80.2± 7.4 Ma, and the resulting thermal history solution (Fig. 8) shows cooling from a maximum paleotemperature >105 °C some time between 100 and 65 Ma. The maximum paleotemperature of 116 °C defined from VR is consistent with this solution, provided that cooling began prior to 75 Ma, which matches the regional framework discussed above. From the track length data a later cooling episode from between 40 and 60 °C is defined within the last 20 Ma, and this can readily be

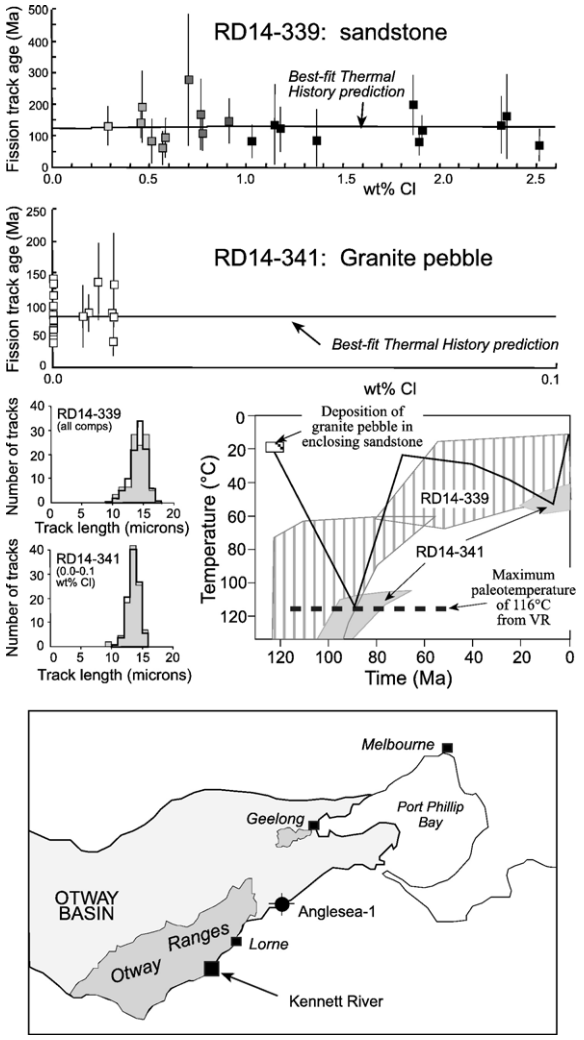

Fig. 8. AFTA data from a granite pebble (RD14-341) and an adjacent sample of volcanogenic sediment (RD14-339) from the shore platform at Kennett River (summary parameters provided in Table 1) and the associated thermal history interpretation (lower right). AFTA data from the volcanogenic sediment provide only broad constraints due to the wider spread of Cl contents, but the results are consistent with results from higher quality data from the granite pebble which define two dominant episodes of cooling, as shown. The variation of fission track age with wt.% Cl and the length distribution predicted from the best-fit history are compared with the measured ages and length distributions in each sample. An independent measure of maximum paleotemperature provided by vitrinite reflectance data is also shown. In the location map, outcropping Early Cretaceous sediments are shown in the darker shading, while the sub-surface extent of the Otway Basin is shown by the lighter shading.

interpreted as representing the regional Miocene exhumation involving erosion of around 1 km of former sedimentary cover beginning at ~10 Ma [10].

AFTA data in sandstone sample RD14-339 are consistent with a similar interpretation (Fig. 8), but do not

provide such good definition of these events due to the dominance of more resistant higher wt.% Cl apatites in this volcanogenic sandstone, which explains the higher fission track age in this sample compared to the granite pebble, RD14-341 (above). In addition, track lengths are spread over a large number of separate compositional groups, which also contributes to the lower resolution of the thermal history solution in this sample. In contrast, 100 track lengths and 20 single grain ages in apatites within a single compositional group (0.0–0.1 wt.% Cl) in sample RD14-341 provide excellent definition of the two dominant paleo-thermal episodes.

The thermal history derived from AFTA and VR in these samples suggests that the mid-Cretaceous maximum paleotemperature of 116 °C experienced by these sediments should have been sufficient to totally anneal all fission tracks in F-rich apatites from these samples, and therefore all of the helium should also have been removed during this episode. Considerable He should also have been lost during the Miocene episode. But measured (U–Th)/He ages in apatites from granite pebble sample RD14-341 (Table 2) are in the range 100 to 160 Ma, older than the supposed resetting event. In contrast, measured (U–Th)/He ages in apatites from the Otway Group sandstone RD14-339 (also listed in Table 2) are generally in the range 20 to 80 Ma. As shown in Fig. 9, measured He ages in sample RD14-339 are broadly consistent with values predicted from the best-fit $T(t)$ solution derived from AFTA data in RD14-341 (the granite pebble) using the He diffusion systematics from Farley (2000), although they show more scatter than expected purely from analytical uncertainties. These ages largely reflect the Miocene episode, following total He loss in the mid-Cretaceous paleo-thermal maximum. But Fig. 9 clearly demonstrates the inconsistency of the measured (U–Th)/He ages in apatites from the granite pebble (RD14-341) with the thermal history framework derived from the remaining AFTA and VR data from this location.

In fact, many of the (U–Th)/He ages measured in apatites from this granite pebble are older than the depositional age of the host sandstone, despite exposure to a maximum paleotemperature ~116 °C in the mid-Cretaceous (ca. 95 Ma). In other words, while fission track data in both granite pebble and volcanogenic sediment are highly consistent and also match the VR data, the He ages from the granite pebble are clearly anomalous, and these apatites have retained He even at paleotemperatures where all fission tracks were totally annealed. The granitic apatites are distinguished from the volcanic apatites by their higher uranium contents (Fig. 9), and on the basis of results discussed in earlier

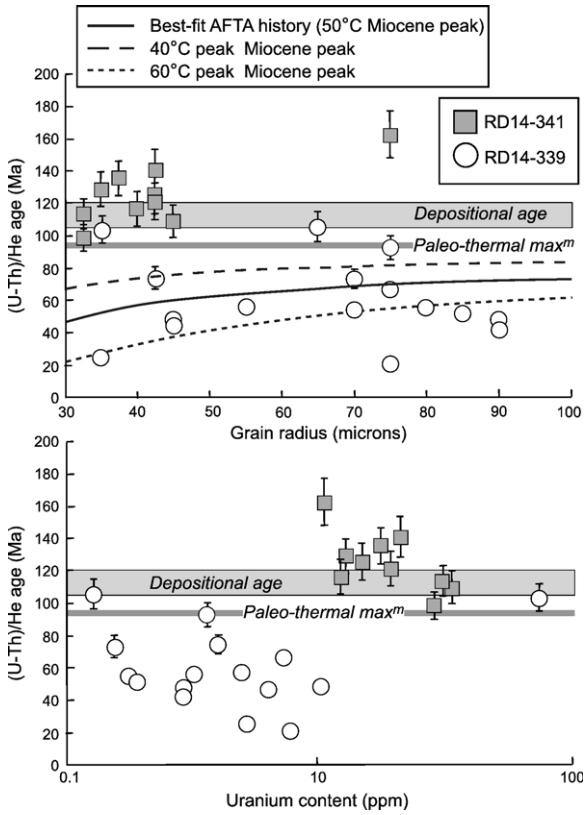

Fig. 9. (U–Th)/He ages in individual apatite grains from granite pebble sample RD14-341 and adjacent volcanogenic sediment sample RD14-339, plotted against grain radius (from Table 2). The depositional age of the volcanogenic sediments and the timing of the dominant cooling episode based on regional data are also shown. Although the two samples have shared a common history involving cooling from a maximum paleotemperature of ~116 °C at ~95 Ma (Fig. 8), the He ages measured in the granitic apatites are much older than those in the sedimentary apatites. In the lower plot, the (U–Th)/He ages from the two samples are plotted against uranium content, illustrating the higher U contents in the granitic apatites. The combined AFTA and (U–Th)/He results from these two samples shows clearly that the increasing discrepancy between measured and predicted He ages shown in Fig. 7 arises because of an increase in He retention as the number of alpha decays from uranium and thorium increases, suggesting a link to radiation damage within the apatite lattice.

sections, the discrepancy between the measured (U–Th)/He ages in the two samples can only be understood if the accumulation of U and Th decays in the apatites within the granite pebble prior to deposition in the sandstone during the Early Cretaceous has in some way rendered the apatites more resistant to He loss (possibly linked to radiation damage?).

These results demonstrate quite clearly that the discrepancy between AFTA and (U–Th)/He data as the number of U and Th decays increases cannot be attributed to an alternative fission track annealing mechanism, as the

AFTA data in both samples are highly consistent with the independent constraints provided by the VR data. In contrast, the (U–Th)/He ages in the higher uranium apatite grains from the granite pebble are clearly anomalously old, suggesting that as the degree of radiation damage within the crystal lattice increases, apatite somehow becomes progressively more retentive of helium. This result is particularly surprising in view of the observation that increasing levels of radiation damage in zircon lead to a reduction in He retentivity [43], emphasising how little is really known of the nature of the processes involved.

10. Implications for routine application of apatite (U–Th)/He dating

The results presented here provide clear evidence that the response of the (U–Th)/He system in apatite progressively departs from published He diffusion systematics as the number of accumulated alpha decays and/or fission events within the crystal lattice increases. Evidence from the Otway Basin granite pebble/volcanogenic sandstone sample pair shows that discrepancies between AFT and (U–Th)/He ages cannot be accounted for by anomalous fission track annealing behaviour, as suggested recently [15], and instead the explanation clearly lies within the (U–Th)/He system.

Because of this effect, for which no known mechanism exists, but which must surely be related in some way to the accumulation of radiation damage within the apatite lattice, use of the published He diffusion systematics [6] is only valid for apatites in which the accumulated radiation dose is similar to that in Durango apatite, in which those systematics were established. As a general guide, for a "typical" basement apatite with uranium and thorium contents around 10 and ~30 ppm, respectively (based on an informal compilation of data from various published (U–Th)/He dating studies), Fig. 7 suggests that only for samples with fission track ages less than ~100 Ma will the published systematics be valid, while practical experience in unpublished studies suggests an upper limit of 50 Ma is more realistic.

As yet, our attempts to measure radiation damage levels in apatite by independent techniques have been unsuccessful, and further efforts in this direction will be required before the effect can be rigorously quantified. In this connection, studies of amorphization due to alpha decay carried out in connection with radioactive waste storage [44] have suggested that alpha decay-induced damage is not stable at upper crustal temperatures over geological timescales. While this may explain our inability to detect such damage, it leaves open the question of how the He retention properties are modified as the number of U and Th decays increases.

We suggest that additional diffusion experiments should be carried out in a range of different apatite species in order to characterise He diffusion in as wide a range of apatites as possible. In addition to the influence of radiation damage, other factors such as composition would also benefit from more detailed investigation. If a systematic effect of radiation damage can be demonstrated and quantified, then modelling of He parameters in order to extract thermal history information from apatites will require incorporation of the changing nature of the material as radiation damage levels increase, before meaningful results can be obtained.

Until such time as this is achieved, we suggest that apatite (U–Th)/He studies should also incorporate apatite fission track data, as well as other low temperature indicators, in order to monitor the (U–Th)/He system response and to guard against the anomalous behaviour described here.

Acknowledgements

PJ thanks the Bureau of Minerals and Petroleum (Government of Greenland) for co-operation and financial support. SPH gratefully acknowledges the National Trust for permission to collect samples from the Snowdonia National Park. PFG and PVC are hugely grateful to Prof. Ken Farley (Division of Geological and Planetary Sciences, California Institute of Technology) for discussions which were of enormous assistance in developing the ideas presented here, and for analytical input with age determinations and diffusion experiments (the results of which will be published elsewhere), all of which contributed significantly to the end-product.

References

[1] R.A. Wolf, K.A. Farley, L.T. Silver, Assessment of (U–Th)/He thermochronometry: the low temperature history of the San Jacinto mountains, California, Geology 25 (1997) 65–68.

[2] M.A. House, B.P. Wernicke, K.A. Farley, T.A. Dumitru, Cenozoic thermal evolution of the central Sierra Nevada, California, from (U–Th)/He thermochronometry, Earth Planet. Sci. Lett. 151 (1997) 167–179.

[3] K.A. Farley, M.E. Rusmore, S.W. Bogue, Post-10 Ma uplift and exhumation of the north Coast Mountains, British Columbia, Geology 29 (2001) 99–102.

[4] P.D. Crowley, P.W. Reiners, J.M. Reuter, G.D. Kaye, Laramide exhumation of the Bighorn Mountains, Wyoming: an apatite (U–Th)/He thermochronology study, Geology 30 (2002) 27–30.

[5] D.F. Stockli, T.A. Dumitru, M.O. McWilliams, K.A. Farley, Cenozoic tectonic evolution of the White Mountains, California and Nevada. GSA Bull. 115 (2003) 788–816.

[6] K.A. Farley, Helium diffusion from apatite: general behaviour as illustrated by Durango fluorapatite, J. Geophys. Res. 105 (B2) (2000) 2903–2914.
[7] M.A. House, K.A. Farley, B.P. Kohn, An empirical test of helium diffusion in apatite: borehole data from the Otway Basin, Australia, Earth Planet. Sci. Lett. 170 (1999) 463–474.
[8] M.A. House, K.A. Farley, B.P. Kohn, Evaluating thermal history models for the Otway Basin, southeastern Australia, using (U-Th)/He and fission track data from borehole apatites, Tectonophysics 349 (2002) 277–295.
[9] P.V. Crowhurst, P.F. Green, P.J.J. Kamp, Appraisal of (U–Th)/He apatite thermochronology as a thermal history tool for hydrocarbon exploration: an example from the Taranaki Basin, New Zealand, AAPG Bull. 86 (2002) 1801–1819.
[10] P.F. Green, P.V. Crowhurst, I.R. Duddy, Integration of AFTA and (U–Th)/He thermochronology to enhance the resolution and precision of thermal history reconstruction in the Anglesea-1 well, Otway Basin, SE Australia, in: P.J. Boult, D.R. Johns, S.C. Lang (Eds.), Eastern Australian Basins Symposium II, Petroleum Exploration Society of Australia, Special Publication, 2004, pp. 117–131.
[11] G.M. Laslett, P.F. Green, I.R. Duddy, A.J.W. Gleadow, Thermal annealing of fission tracks in apatite 2. A quantitative analysis, Chem. Geol., Isot. Geosci. Sect. 65 (1987) 1–13.
[12] R.A. Ketcham, R.A. Donelick, W.D. Carlson, Variability of apatite fission-track annealing kinetics: III. extrapolation to geological timescales, Am. Mineral. 84 (1999) 1235–1255.
[13] C. Persano, F.M. Stuart, P. Bishop, D.N. Barfod, Apatite (U–Th)/He age constraints on the development of the Great Escarpment on the southeastern Australian passive margin, Earth Planet. Sci. Lett. 219 (2002) 1–12.
[14] J.A. Spotilla, G.C. Bank, P.W. Reiners, C.W. Naeser, N.D. Naeser, B.S. Henika, Origin of the Blue Ridge escarpment of Eastern North America, Basin Res. 16 (2004) 41–63.
[15] B.W.H. Hendriks, T.F. Redfield, Apatite fission track and (U–Th)/He data from Fennoscandinavia: an example of underestimation of fission track annealing in apatite, Earth Planet. Sci. Lett. 236 (2005) 443–458.
[16] P. Soderlund, J. Juez-Larre, L.M. Page, T.J. Dunai, Extending the time range of (U–Th)/He thermochronometry in slowly cooled terranes: Paleozoic to Cenozoic exhumation history of southeast Sweden, Earth Planet. Sci. Lett. 239 (2005) 266–275.
[17] P.F. Green, I.R. Duddy, K.A. Hegarty, Quantifying exhumation from apatite fission-track analysis and vitrinite reflectance data: precision, accuracy and latest results from the Atlantic margin of NW Europe, in: A.G. Doré, J. Cartwright, M.S. Stoker, J.P. Turner, N. White (Eds.), Exhumation of the North Atlantic Margin: Timing, Mechanisms and Implications for Petroleum Exploration, Geological Society Special Publication, vol. 196, 2002, pp. 331–354.
[18] W.B. Harland, R.L. Armstrong, A.V. Cox, L.E. Craig, A.G. Smith, D.G. Smith, A Geologic Time Scale 1989, Cambridge University Press, 1989.
[19] R.F. Galbraith, G.M. Laslett, Statistical methods for mixed fission track ages, Nucl. Tracks 21 (1993) 459–470.
[20] A.J.H. Hurford, P.F. Green, The zeta age calibration of fission-track dating, Chem. Geol., Isot. Geosci. Sect. 1 (1983) 285–317.
[21] P.F. Green, K. Thomson, J.D. Hudson, Recognising tectonic events in undeformed regions: contrasting results from the Midland Platform and East Midlands Shelf, Central England, J. Geol. Soc. (Lond.) 158 (2001) 59–73.
[22] A.G.C.A. Meesters, T.J. Dunai, Solving the production–diffusion equation for finite diffusion domains of various shapes Part II. Application to cases with α-ejection and nonhomogenous distribution of the source, Chem. Geol. 186 (2002) 347–363.
[23] J.A. Chalmers, T.C.R. Pulvertaft, Development of the continental margins of the Labrador Sea: a review, in: R.C.L. Wilson, R.B. Withmarsh, B. Taylor, N. Froitzheim (Eds.), Non-volcanic Rifting of Continental Margins: A Comparison of Evidence from Land and Sea, Geol. Soc. London Spec. Publ., vol. 187, 2001, pp. 77–105.
[24] P. Japsen, J.M. Bonow, P.F. Green, J.A. Chalmers, K. Lidmar-Bergström, Elevated, Passive Continental Margins: Long-term Highs or Neogene Uplifts? Earth Planet. Sci. Lett. 248 (2006) 315–324.
[25] F.W. McDowell, W.C. McIntosh, K.A. Farley, A precise ^{40}Ar–^{39}Ar reference age for the Durango apatite (U–Th)/He and fission-track dating standard, Chem. Geol. 214 (2005) 249–263.
[26] U. Weber, B.P. Kohn, A.J.W. Gleadow, D.R. Nelson, Low temperature Phanerozoic history of the Yilgarn Craton, Western Australia, Earth Planet. Sci. Lett. 239 (2005) 266–275.
[27] P.A. Cawood, A.A. Nemchin, Provenance record of a rift basin: U/Pb ages of detrital zircons from the Perth Basin, Western Australia, Sediment. Geol. 134 (2000) 209–234.
[28] P.F. Green, Comparison of zeta calibration baselines for fission-track dating of apatite, zircon and sphene, Chem. Geol., Isot. Geosci. Sect. 58 (1985) 1–22.
[29] W. Compston, SIMS U–Pb zircon ages for the Upper Devonian Snobs Creek and Cerberean volcanics from Victoria, with age uncertainty based on UO_2/UO v. UO/U precision, J. Geol. Soc. (Lond.) 161 (2004) 223–228.
[30] R.A.F. Cas, G.J. O'Halloran, J.A. Long, A.H.M. VandenBerg, Middle Devonian to Carboniferous: late to post-tectonic sedimentation and magmatism in an arid continental setting, in: W. Birch (Ed.), Geology of Victoria, Chapter 6, Special Publication, vol. 23, Geological Society of Australia, 2003.
[31] T.A. Dumitru, K.C. Hill, D.A. Coyle, I.R. Duddy, D.A. Foster, A.J.W. Gleadow, P.F. Green, B.P. Kohn, G.M. Laslett, P.J. O'Sullivan, Fission track thermochronology: application to continental rifting of south-eastern Australia, APEA J. 10 (1991) 131–142.
[32] L.P. Black, B.L. Gulson, The age of the Mud Tank Carbonatite, Strangways Range, Northern Territory, BMR J. Aust. Geol. Geophys. 3 (1978) 227–232.
[33] P.W. Haines, M. Hand, M. Sandiford, Palaeozoic synorogenic sedimentation in central and northern Australia: a review of distribution and timing with implications for the evolution of intracontinental orogens, Aust. J. Earth Sci. 48 (2001) 911–928.
[34] P.R. Tingate, Apatite fission track analysis of the Pacoota and Stairway Sandstones, Amadeus basin, central Australia, BMR Bull. 236 (1991) 525–540.
[35] P.R. Tingate, J.F. Lindsay, S.J. Marshallsea, Impact structures as potential petroleum exploration targets: Gosses Bluff, a Late Jurassic example In Central Australia, AGSO J. Aust. Geol. Geophys. 16 (1996) 529–552.
[36] B.P. Kohn, personal communication.
[37] S.P. Holford, J.P. Turner, P.F. Green, Reconstructing the Mesozoic–Cenozoic exhumation history of the Irish Sea basin system using apatite fission-track analysis and vitrinite reflectance data, in: A.G. Doré, B.A. Vining (Eds.), Petroleum Geology: North West Europe and Global Perspectives — Proceedings of the 6th Petroleum Geology Conference, Geological Society, London, 2003, pp. 1095–1107.

[38] P.G. Fitzgerald, S.L. Baldwin, L.E. Webb, P.B. O'Sullivan, Interpretation of (U–Th)/He single grain ages from slowly cooled crustal terranes: a case study from the Transantarctic Mountains of southern Victoria Land, Chem. Geol. 225 (2006) 91–120.
[39] I.R. Duddy, Mesozoic: a time of change in tectonic regime, in: W. Birch (Ed.), Geology of Victoria, Chapter 9, Special Publication, vol. 23, Geological Society of Australia, 2003.
[40] I.R. Duddy. The Otway Basin: Thermal, structural, tectonic and hydrocarbon generation histories. In, Finlayson, D.M. (compiler), NGMA/PESA Otway Basin Symposium, Melbourne, 20 April 1994: extended abstracts, AGSO Record 1994/14, 35–42.
[41] I.R. Duddy, Focussing exploration in the Otway Basin: understanding timing of source rock maturation, APPEA J. 37 (1997) 178–191.
[42] A.J.W. Gleadow, J.F. Lovering, Fission track geochronology of King Island, Bass Strait, Australia: relationship to continental rifting, Earth Planet. Sci. Lett. 37 (1978) 429–437.
[43] P.W. Reiners, Zircon (U–Th)/He Thermochronometry, Rev. Mineral. Geochem. 58 (2005) 151–179.
[44] W.J. Weber, R.C. Ewing, A. Meldrum, The kinetics of alpha-decay induced amorphization in zircon and apatite containing weapons — grade plutonium or other actinides, J. Nucl. Mater. 250 (1997) 147–155.
[45] K.A. Farley, R.A. Wolf, L.T. Silver, The effects of long alpha-stopping distances on (U–Th)/He ages, Geochim. Cosmochim. Acta 60 (1996) 4223–4229.